THE UNIVERSITY OF SYDNEY

SCHOOL OF CIVIL ENGINEERING

STIFFNESS REDUCTION OF COLD-FORMED STEEL STRUCTURES SUBJECT TO SECTIONAL BUCKLING AND YIELDING

RESEARCH REPORT R971

K J R RASMUSSEN

December 2022

ISSN 1833-2781

Copyright Notice

School of Civil Engineering, Research Report R971
Stiffness reduction of cold-formed steel structures subject to sectional buckling and yielding
K J R Rasmussen MScEng PhD DEng
December 2022

ISSN 1833-2781

This publication may be redistributed freely in its entirety and in its original form without the consent of the copyright owner.

Use of material contained in this publication in any other published works must be appropriately referenced, and, if necessary, permission sought from the author.

Published by:
School of Civil Engineering
The University of Sydney
Sydney NSW 2006
Australia

Abstract

The paper develops a stiffness reduction factor to be used in geometric nonlinear beam-element type elastic analysis of cold-formed steel structures. The factor accounts for the reduction in flexural and warping torsion rigidities resulting from local and distortional buckling as well as residuals stresses, as particular to cold-formed steel structures. The purpose of applying the factor is to accurately account for the geometric second order effects when predicting the internal distributions of moments of cold-formed steel structural frames. The stiffness reduction factor arising from local and distortional buckling is first determined followed by the stiffness reduction factor caused by residual stresses. Subsequently, the two effects are combined in a single expression is a format suitable for incorporation in the North American specification for cold-formed steel structures, AISI-S100.

Keywords: Cold-formed steel, local buckling, distortional buckling, residual stress, stiffness reduction

Table of Content

Abstract	3
Keywords	3
1 Introduction	5
2. Slenderness reduction produced by geometric imperfections	6
3. Slenderness reduction produced by residual stresses and yielding	12
4. Slenderness reduction factor (τ_b)	14
5. Conclusions	16
References	17

1. Introduction

Hot-rolled and fabricated steel frames composed of slender cross-sections are prone to fail by interaction of local buckling and buckling of component load carrying members, including columns and beams. In the case of cold-formed steel (CFS) frames, the cross-section may buckle in local and/or distortional modes, collectively referred to as sectional buckling modes. Figure 1 shows the sectional buckling modes of plain and lipped channel sections. As is well-known [1-3], sectional buckling reduces the stiffness of the cross-section, leading to the accelerated growth of flexural and/or flexural-torsional buckling deformations of the member and a reduced ultimate capacity. A general theory for calculating the buckling load of a sectionally buckled member has been established [4] and applied to doubly- [4], singly- [5, 6] and point-symmetric [7] columns, as well as to beams and beam-columns [8].

a) Local buckling b) Local buckling c) Distortional buckling

Fig. 1: Sectional buckling modes of plain (unlipped) and lipped channel section

Fig. 2a shows the reductions in rigidities for minor axis bending (EI_y), major axis bending (EI_x) and warping torsion (EI_ω) as the result of local buckling of a plain channel section in compression [5]. The loss of stiffness commences prior to the local buckling load (P_l) because of geometric imperfections and is a function of the level of imperfection and yield stress relative to the sectional buckling load. As shown in Fig. 2a, the larger the imperfection (w_o), the faster the loss of stiffness under increasing load.

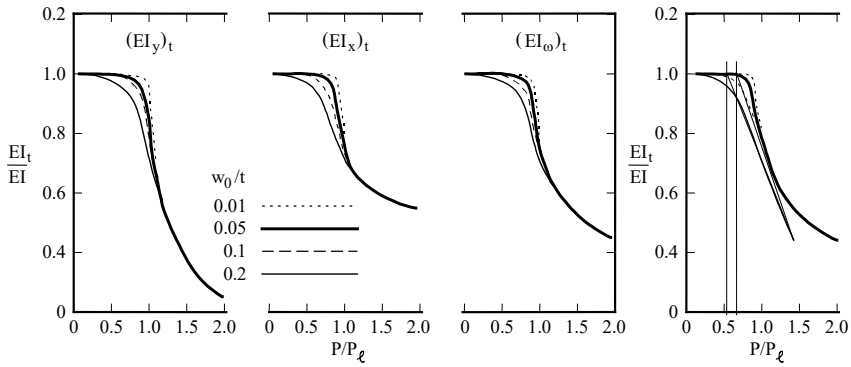

Fig. 2: Inelastic stiffness reduction of plain channel section in compression; a) minor axis bending $(EI_y)_t$, major axis bending $(EI_x)_t$, warping torsion $(EI_\omega)_t$; b) linear fits to stiffness curves

Residual stresses produce premature yielding in parts of the cross-section and are known also to reduce stiffness [9]. In hot-rolled and welded sections, residual stresses are caused by the non-uniform cooling of the cross-section, whereas in cold-formed steel sections, residual stresses arise from the cold-rolling or brake-pressing process and are dominated by through-thickness variations of stress [10].

In the design of steel structural frames, the stiffness reductions arising from sectional buckling and/or residual stresses must be accounted for in determining the distribution of internal actions. In applying the direct analysis method of design of the 2016 versions of the American specifications for hot-rolled [11] and cold-formed [12] steel structures, this is achieved by applying the stiffness reduction factor $\tau_b \leq 1$,

$$\tau_b = \begin{cases} 1 & \text{for} \quad \frac{P}{P_y} \leq 0.5 \\ 4\frac{P}{P_y}\left(1 - \frac{P}{P_y}\right) & \text{for} \quad \frac{P}{P_y} > 0.5 \end{cases} , \tag{1}$$

to the stiffness of all members whose stiffnesses contribute to the stability of the structure, where P is the compressive axial force and $P_y = AF_y$ is the yield load. While this expression accounts for the premature yielding in parts of the cross-section induced by residual stresses, it does not account for the stiffness reduction caused by sectional buckling. In the 2022 version of the AISC-360 Specification [13], P_y was changed to the section capacity $P_{ns} = A_eF_y$ to account for the combined effects of yielding and local buckling.

As similar change is required for the AISI-S100 Specification for CFS structures. However, unlike hot-rolled steel frames, sectional buckling of CFS frames includes both local and distortional modes, both of which have associated stiffness reductions similar to those shown in Fig. 2a, and may occur well before reaching the sectional buckling strength, depending on the slenderness of the cross-sections of the main load carrying members. Also, the stiffness reduction induced by residual stresses is different as the residual stress distribution in CFS sections bears no resemblance to those of hot-rolled and welded sections. The purpose of this paper is to derive an expression for τ_b that accounts for the combined effects of sectional buckling and residual stress on the stiffness of CFS members.

2. Slenderness reduction produced by geometric imperfections

2.1. Modelling the effect of geometric imperfections

The stiffness reduction curves shown in Fig. 2a were obtained from inelastic post-buckling analyses of a plain channel section with length equal to the local buckling half-wavelength, referred to as a locally buckled cell, and imperfection in the shape of the local buckling mode [5]. Similar stiffness reduction curves can be obtained for other types of cross-sections, including sections for which the critical sectional buckling mode is the distortional mode. While flexural and warping stiffness reduction curves are not currently available for the distortional buckling mode, a study of the distortional buckling behaviour of lipped channels [14] demonstrated that the elastic axial post-distortional buckling stiffness was about 60% of the initial value, i.e. $EA_t / EA \approx 0.6$. The implied reduction of about 40% is similar to that shown for major axis bending ($(EI_x)_t / EI_x$) in Fig. 2a but less than reductions for minor axis bending ($(EI_y)_t / EI_y$) and warping torsion ($(EI_\omega)_t / EI_\omega$) also shown in Fig. 2a. As the axial stiffness is generally slightly more reduced than the flexural and warping stiffnesses, this result implies that the stiffness reduction curves shown in Fig. 2a may conservatively be assumed to also apply to distortional buckling.

If the stiffness reduction shown in Fig. 2a is applied to the full length of the member, the implication is that the shape of the sectional imperfection (local or distortional) is a repeated series of buckles, as shown in Fig. 3, i.e. it is assumed the shape of the imperfection is the sectional buckling mode of the member.

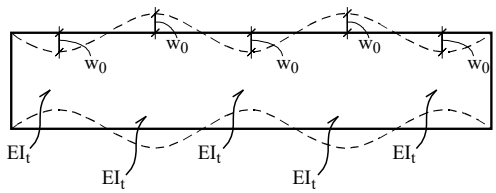

Fig. 3: Pure sectional mode imperfection with five half-wavelengths

However, the sectional buckling mode of the member does not represent actual distributions of sectional imperfections. Rather, it is recognised that the distributions of local and distortional geometric imperfections are random. Also, comparatively large geometric imperfections are often localised in a relatively small part of the member, as exemplified in Fig. 4a for a plain channel section. This raises the question about how the stiffness is reduced when the magnitude of the imperfection varies along the length. To answer this question, consider the idealised representation of the imperfection shown in Fig. 4b, in which the stiffness is reduced from EI to EI_l over the length (l) of the localised imperfection and the remaining length of the member is geometrically perfect with full stiffness (EI). Note that a plain channel is shown by way of example; it could equally well have been a lipped channel with a dominant distortional imperfection.

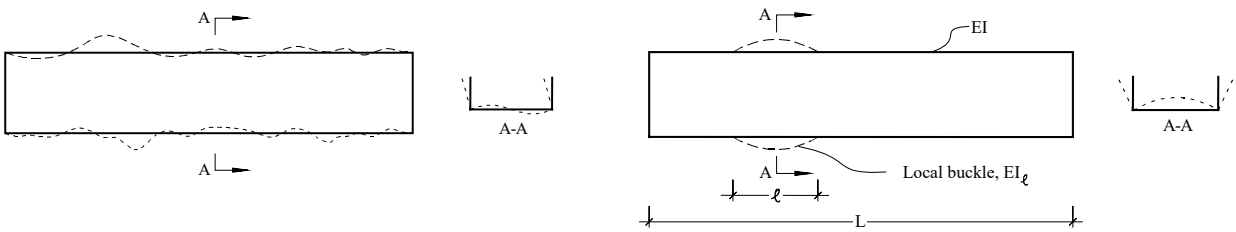

a) Typical random geometric imperfection b) Idealised geometric imperfection

Fig. 4: Typical random geometric imperfections of plain channel section and idealisation

A simple model of the idealised member is shown in Fig. 5a where moments are applied at the ends to create a state of uniform moment.

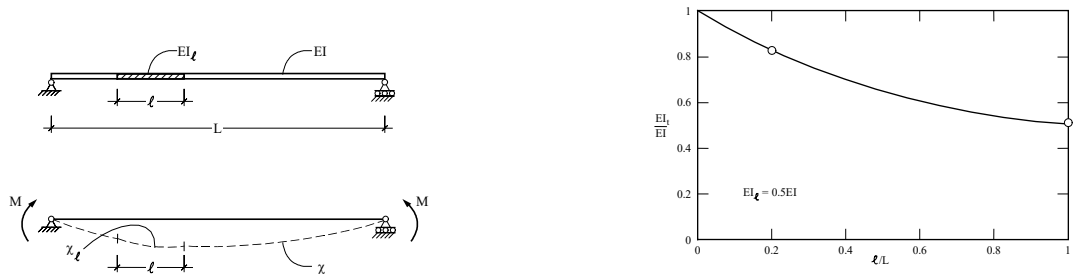

a) Localised geometric imperfection b) Stiffness reduction as function of length of imperfection, $EI_l = 0.5EI$

Fig. 5: Beam with localised imperfection under uniform moment and resulting stiffness reduction

The moment (M) induces curvatures κ_l and κ over the lengths with and without imperfection, respectively. Calculating the average moment curvature $\kappa_{av} = \int \kappa(\mathbf{z})\, \mathbf{dz}/L$, the rigidity ($EI_t = M/\kappa_{av}$) can be obtained as,

$$\frac{EI_t}{EI} = \frac{1}{1+\left(\frac{EI}{EI_l}-1\right)\frac{l}{L}} \tag{2}$$

The relationship is plotted in Fig. 5b for $EI_l = 0.5EI$ and demonstrates that the stiffness reduction is nearly linear with the length of the imperfection. In other words, the stiffness reduction is the average of the stiffness reductions in different parts of the member. It follows that a large localised imperfection concentrated over a short length of the member does not significantly reduce the stiffness.

The model can be refined to consider a member with a large imperfection over the length l and a small imperfection elsewhere, also with the length l of each halfwave, as shown in Fig. 6a. Because of the difference in the magnitude of the imperfections, the stiffness reduces at different rates in the different parts of the beam, as shown in Fig. 2a. Simplifying the stiffness reduction curves by linear curves, as shown in Fig. 2b, the stiffness reduction starts at an increasingly lower load ($P/P_l < 1$) for increasing amplitude of imperfection, where P_l is the local buckling load. Thus, the stiffness reductions in the parts of the beam with small and large magnitudes of imperfection can be idealised as shown in Fig. 6b, where for simplicity, the stiffness reduction is assumed to be elastic with a post-buckling stiffness of half of the initial stiffness.

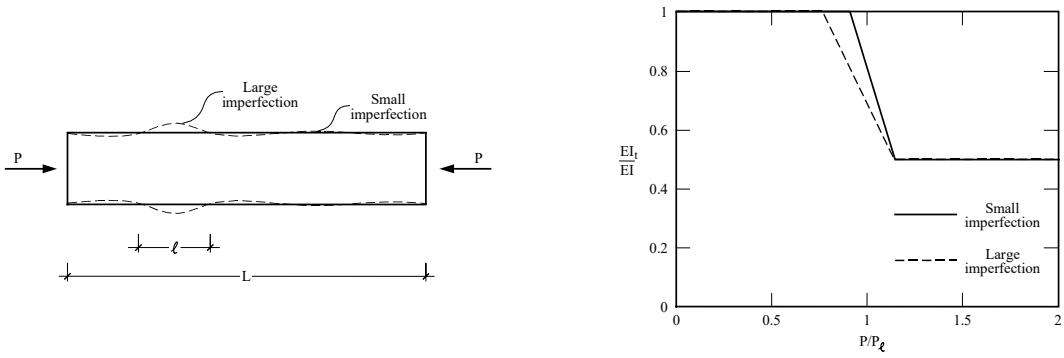

a) Member with small and large imperfections

b) Stiffness reduction in respective lengths, $EI_l = 0.5EI$

Fig. 6: Refined model with small and large imperfections

The solution is obtained using Eq. (2), except that the stiffness in each part of the member is calculated at the particular level of axial force, as per Fig. 6b. The resulting stiffness reduction curves are shown in Fig. 7. It follows that the effect of the large imperfection present over a relatively small length is to initiate the stiffness reduction at a small axial force. However, the rate of reduction remains small until the stiffness of the remaining length of the member starts reducing. It is again seen that the stiffness reduction is dominated by the reduction of the part of the member with the predominant level of imperfection.

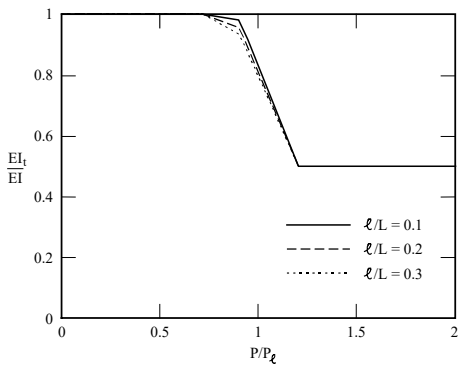

Fig. 7: Stiffness reduction of member with small and large imperfections, $EI_l = 0.5EI$

2.2. Imperfection data and amplitudes

Evidently, the stiffness reduction is a function of the levels of imperfection in typical members. While numerous papers contain measured imperfections of specimens of reported series of tests, most papers simply report the maximum imperfections measured at any point in a given member. Few papers report lengthwise distributions and few report statistics. Exceptions are the studies by Schafer & Pekoz [15] and Zeinoddini and Schafer [16], both concerning lipped channel sections. Among other data, the

former study provides statistical data for the *magnitudes* of local and distortional geometric imperfections, as defined in [15], but not statistical data for the lengthwise distribution of imperfections. It was reported that the 50% Cumulative Distribution Function (CDF) values of $w_{ol}/t=0.34$ and $w_{od}/t=0.94$ were obtained for the local and distortional geometric imperfection amplitudes, respectively, where t is the thickness. These CDF-values represent typical values of large localised imperfections, as illustrated in Fig. 4a, and not the predominant level of imperfection.

In [16], the measured imperfections were expanded transversely in the buckling modes of the section and lengthwise in Fourier series following the approach set out in [17], which expands the measured imperfection in the buckling modes of the member. For each Fourier term (or number of half-waves, m), the amplitude (S_f) of each transverse mode, including the local and distortional modes, was reported, see Fig. 8. In construction, the lengths of CFS columns are such that m=4 distortional buckles typically form along the length, whereas the number of local buckles may be closer to around m=20. It follows from Fig. 8b that the amplitude of the distortional imperfection is about $S_f/t=0.2$. This is the amplitude of a "pure" distortional imperfection in the shape of the distortional buckling mode, as exemplified in Fig. 3. The imperfection in this shape is likely to dominate the response of the member, when buckling occurs elastically, and as such represents the predominant level of imperfection. Because of the relatively small number of half-waves, imperfection components in neighbouring modes (e.g. m=3 or m=5) are unlikely to contribute greatly to the response, and by implication the stiffness reduction, because their corresponding buckling loads are higher than that for m=4. Importantly, the amplitude of the regularly distributed distortional buckling imperfection emerges as $w_{od}/t=0.20$. This is about one fifth of the 50% CDF-value of maximum distortional geometric imperfection reported in [15].

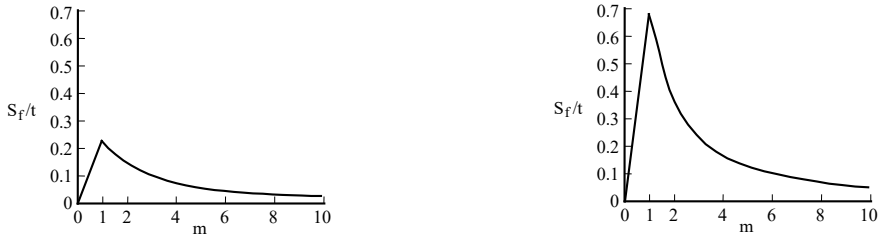

a) Local imperfection b) Distortional imperfection

Fig. 8: Imperfection amplitudes against number of half-wavelengths

According to Fig. 8a, the amplitude of the local buckling imperfection is about $S_f/t=0.025$, corresponding to, say, m=20. However, in this case, because the buckling loads of neighbouring modes (say m=18,19,21,22) are close to that of m=20, (as their half-wavelengths are close), imperfection components of neighbouring modes are likely to also affect the stiffness reduction [17]. As an approximate calculation, it may be assumed that local modes with half-wavelengths within ±10% of the critical mode will contribute, which translates to the minimum and maximum numbers of halfwaves of m/1.1 and m/0.9, respectively, i.e. for m=20, modes with m=18, 19, 20, 21 and 22 may be assumed to contribute to the stiffness reduction. It is unknown how their contributions combine but guided by frequency analysis, we may assume their contributions can be added using the Square Root of Sum of Squares calculation. Because of the flatness of the S_f/t-curve at large values of m, the amplitude of all modes can be taken as $S_f/t=0.025$, and so the combined effect is $S_f/t=\sqrt{5}\times0.025\approx0.05$. We may use this value ($w_{ol}/t=0.05$) as the amplitude of the regularly distributed local buckling imperfection illustrated in Fig. 3, which represents the predominant level of imperfection. The value is about on seventh of the 50% CDF-value of maximum local geometric imperfection reported in [15].

2.3. Initiation points (a_l, a_d) of stiffness reduction

The stiffness reduction curves shown in Fig. 2a display a gradual change of stiffness, the rate of which depends on the magnitude of imperfection, and is slow initially. The curves may be simplified using linear fits through the steeply descending parts of the curves, as shown in Fig. 2b, such that the stiffness reduction commences at the intersection of the fitted linear curve and the horizontal line ($EI_t/EI=1$) representing full stiffness. The loads corresponding to this intersection point are referred to as a_lP_l and a_dP_d for local and distortional buckling, respectively.

Suitable values of a_l can be obtained from the linear fits to the $(EI)_t/EI$ vs P/P_l curves, as demonstrated in Fig. 2b. The curves shown in Fig. 2a were obtained for plain channel sections and indicated the stiffness reduction for local buckling. As mentioned in Section 2.1, similar curves are not available for distortional buckling but may be assumed to be similar. The values of the cut-off (a_l) for each assumed value of imperfection are plotted in Fig. 9 for the flexural rigidities about the x- and y-axes, indicating a steeper drop in stiffness for the minor y-axis. Trendlines are also fitted through the calculated values of a_l. Assuming the curves shown in Fig. 9 are valid for both local and distortional buckling, the values for a_l and a_d are readily read off the curves for the imperfection amplitudes previously obtained ($w_{ol}/t=0.05$ and $w_{od}/t=0.20$), as summarised in Table 1. Average values for minor and major axis bending can be obtained, suggesting $a_l = 0.9$ and $a_d = 0.7$.

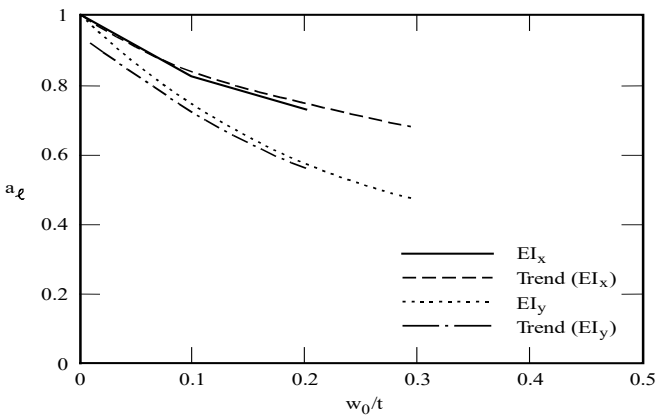

Fig. 9: Relationship between a_l and imperfection magnitude

Table 1: a_l and a_d for plain and lipped channel sections.

	Local (a_l)	Distortional (a_d)
Plain channels (EI_x)	0.90	0.75
Plain channels (EI_y)	0.85	0.60
Plain channels	0.9	0.7
Lipped channels	0.9	0.8

The stiffness reduction for lipped channels and other common CFS cross-sections with lip stiffeners can be assumed to be less severe than for plain channels, especially for bending about the minor y-axis. Hence, the more pertinent values of $a_l = 0.9$ and $a_d = 0.8$ may be assumed for lipped channel sections and other CFS cross-sections which do not rely primarily on unstiffened elements to provide flexural and torsional stiffness.

2.4. Stiffness reduction curve

The inelastic stiffness reduction curves shown in Fig. 2a were obtained for a material with stress-strain curve defined by the Ramberg-Osgood expression (Eq. (3)) with an exponent (n) equal to 8 [5], representative of materials with significant softening, such as austenitic stainless steel alloys and work hardenable aluminium alloys.

$$\varepsilon = \frac{\sigma}{E} + 0.002\left(\frac{\sigma}{F_y}\right)^n \tag{3}$$

Additional stiffness reduction curves are shown in Fig. 10 for materials with values of n = 5, 25 and ∞, where n = 25 and n = ∞ are representative of CFS with low levels of residual stress and ordinary carbon steel with sharp transition from elastic state to the yield plateau, respectively, [5]. It follows that the stiffness reduction curves may be approximated by linear or parabolic curves, as shown in Fig. 11a, where, herein, a linear transition curve is chosen.

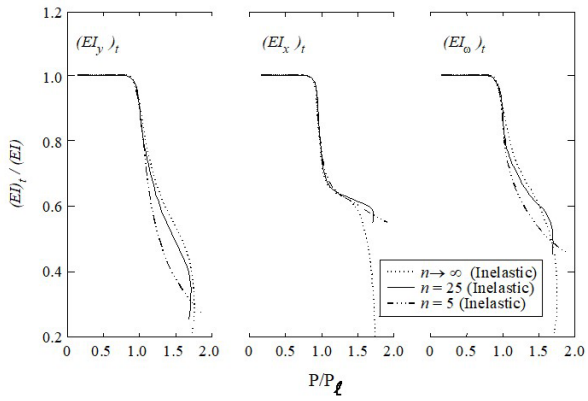

Fig. 10: Inelastic stiffness reduction of plain channel section in compression; n = 5, 25, ∞; w_o/t = 0.02 [5]

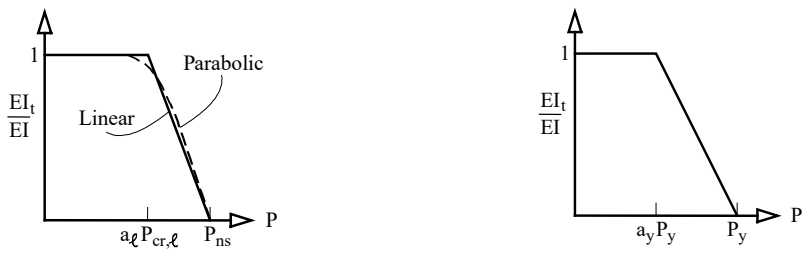

a) Slender cross-section b) Stocky cross-section

Fig. 11: Inelastic stiffness reduction curves; a) slender cross-section (local buckling), b) stocky cross-section

The linear stiffness reduction commences at the load $a_l P_{cr,l}$, where $P_{cr,l}$ is used in lieu of P_l to emphasise it refers to elastic critical buckling. The stiffness reduction transitions to zero at the section capacity (P_{ns}), which is the strength of a short length of member and accounts for the effect of sectional buckling and yielding. Note that while the stiffness curves shown in Fig. 11a were obtained from those shown for local buckling in Fig. 10, similar curves will be assumed to also apply to distortional buckling for which accurate stiffness reduction curves of the kind shown in Fig. 10 are not available.

The section capacity (P_{ns}) is readily obtained from a design specification, such as the Direct Strength Method included in AISI-S100 Specification [12]. Considering stiffness reduction caused by either local or distortional buckling, the linear stiffness reduction can be expressed as,

$$\frac{EI_t}{EI} = \begin{cases} 1 & \text{for} \quad \frac{P}{P_{ns}} \leq a_s \\ \frac{1-\frac{P}{P_{ns}}}{1-a_s} & \text{for} \quad \frac{P}{P_{ns}} > a_s \end{cases} \tag{4}$$

where a_s is the sectional buckling cut-off, taken as a_l or a_d depending on whether local buckling ($a_l P_{cr,l} < a_d P_{cr,d}$) or distortional buckling ($a_d P_{cr,d} < a_l P_{cr,l}$) initiates the stiffness reduction, respectively.

3. Slenderness reduction produced by residual stresses and yielding

3.1. Residual stresses in CFS sections

Cold-formed steel sections feature residual stresses as a result of the cold-forming process. The two main sources of residual stress are the coiling-uncoiling of the steel strip prior to roll-forming and the roll-forming process itself. The residual stresses of sections brake-pressed from flat sheets of steel are significantly lower than those of cold-rolled sections and are concentrated near the brake-pressed corners. Irrespective of the forming process, relatively stocky CFS sections may yield prematurely and lose stiffness because of residual stresses prior to reaching the sectional buckling load ($a_l P_{cr,l}$ or $a_d P_{cr,d}$).

There are three main components of residual stress in cold-rolled sections, viz. the membrane, bending and layering components [18]. The three components exist in both the longitudinal and transverse directions, implying a total of six residual stress components. Of these, the membrane components (constant through the thickness) are usually small and ignored, whereas the bending components (linear variation from a positive to a negative maximum at the surfaces) and the layering components (multi-linear variation through the thickness) have non-negligible values. Both the bending and layering residual stress components are present in testing tensile coupons cut from cold-rolled sections, and give rise to gradual yielding of the stress-strain curve. A simple approach to determining the factor to account for the stiffness reduction caused by residual stress-induced premature yielding is to calculate the reduction as E_t/E ($=EI_t/EI$) where E_t is the tangent of the stress-strain curve.

3.2. Stress-strain curve

A method is presented in [19] for constructing the stress-strain curve of CFS sections when the bending and layering residual stress components are known. It is shown [19] that the accurate stress-strain curve incorporating all components of residual stress can be closely approximated by only accounting for the usually dominant longitudinal bending component. On this assumption, using the analysis described in [19], the stress (σ) vs strain (ε) curve can be expressed as,

$$\frac{\sigma}{F_y} = \begin{cases} \frac{E}{F_y}\varepsilon & \text{for} \quad \varepsilon < (1-a)\frac{F_y}{E} \\ -\frac{1}{4a}\left(\frac{E}{F_y}\right)^2 \varepsilon^2 + \frac{1+a}{2a}\left(\frac{E}{F_y}\right)\varepsilon - \frac{(1-a)^2}{4a} & \text{for} \quad (1-a)\frac{F_y}{E} \leq \varepsilon \leq (1+a)\frac{F_y}{E} \\ 1 & \text{for} \quad \varepsilon > (1+a)\frac{F_y}{E} \end{cases} \tag{5}$$

where F_y is the yield stress, E is the elastic modulus and a is the ratio of the longitudinal bending residual stress component to the yield stress,

$$a = \frac{\sigma_b}{F_y}\,. \tag{6}$$

Figure 12 shows stress-strain curves computed using Eq. (5) for E=200,000MPa, F_y=300MPa and F_y=550MPa, and a=0.25 and a=0.5. The stress-strain curves are evidently highly dependent on the chosen value of a. Research on cold-formed steel tubular sections [18, 20] suggests the longitudinal bending residual stress is typically half the yield stress, i.e. a=0.5. However, arguably, this value may be deemed too high for common cold-rolled open CFS sections.

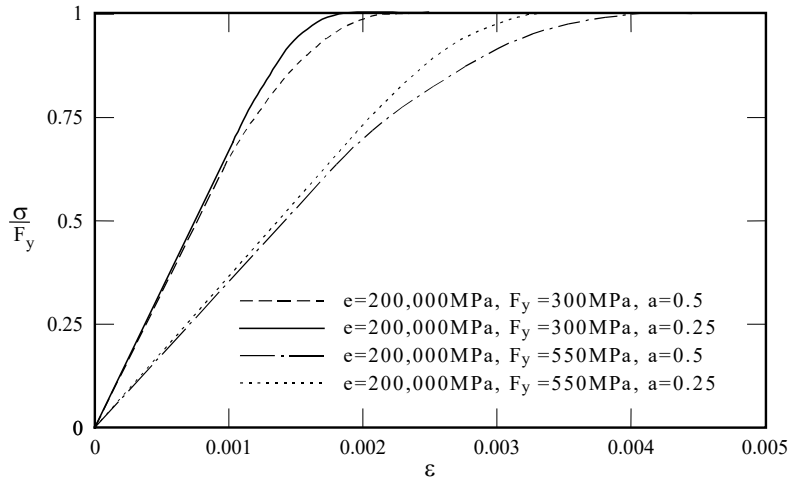

Fig. 12: Stress-strain curves for varying levels of bending residual stress and yield stress

To determine a suitable value of a (Eq. (6)) for open CFS sections, it is observed that the stress-strain curves shown in Fig. 12 resemble Ramberg-Osgood curves, i.e. curves defined by Eq. (3), in which the exponent n determines the degree of gradual yielding. Fitting Ramberg-Osgood curves to stress-strain curves for open CFS sections typically results in n-values between 10 and 30, depending on the level of through-thickness residual stress. This result may be used to determine values of a by defining the proportionality stress (σ_p) as the 0.01% proof stress, which is common practice, equating the proportionality stress to F_y-σ_b, and then calculating a using Eq. (6).

It follows from Eq. (3) that the proportionality stress (σ_p) is related to the plastic component (ε_p^p) of the corresponding strain through,

$$\varepsilon_p^p = 0.0001 = 0.002\left(\frac{\sigma_p}{F_y}\right)^n. \tag{7}$$

Solving this equation for n=10, 20 and 30 produces values of σ_p/F_y of 0.74, 0.86 and 0.90, respectively. Using σ_p=F_y-σ_b, these values imply values of a of 0.26, 0.14 and 0.10, respectively. Conservatively, the value of a=0.25 may be assumed for open CFS sections.

3.3. Stiffness reduction curve

Having obtained the stress-strain curve, the tangent modulus (E_t) is readily obtained,

$$E_t = \frac{d\sigma}{d\varepsilon} \tag{8}$$

where σ is given by Eq. (5). The following equation is obtained,

$$\frac{E_t}{E} = \begin{cases} 1 & \text{for} \quad \varepsilon < (1-a)\frac{F_y}{E} \\ -\frac{1}{2a}\frac{E}{F_y}\varepsilon + \frac{1+a}{2a} & \text{for} \quad (1-a)\frac{F_y}{E} \le \varepsilon \le (1+a)\frac{F_y}{E} \\ 0 & \text{for} \quad \varepsilon > (1+a)\frac{F_y}{E} \end{cases} \tag{9}$$

Thus, expressed in terms of strain, the stiffness reduces linearly between the elastic and fully plastic ranges. To express the stiffness reduction in terms of stress, Eq. (5) is first inverted to express strain in terms of stress, and the resulting expression for the strain (ε) is then substituted into Eq. (9), producing:

$$\frac{E_t}{E} = \begin{cases} 1 & \text{for} \quad \frac{\sigma}{F_y} < 1-a \\ \sqrt{\frac{1-\frac{\sigma}{F_y}}{a}} & \text{for} \quad 1-a \le \frac{\sigma}{F_y} \le 1 \end{cases} . \tag{10}$$

The stiffness reduction thus obtained is shown as solid curves in Fig. 13 for a=0.25 and a=0.5. Conservative linear approximations passing through the end points of the nonlinear parts of the stiffness curves are shown using dashes lines. Linear approximations that produce approximate best fits are also shown using dotted lines. The linear best fit for a=0.25 emerges as a possible solution for E_t/E to account for the stiffness reduction caused by residual stress-induced premature yielding. In terms of applied load ($P=A\sigma$) and yield load ($P_y=AF_y$), the stiffness reduction may be expressed as,

$$\frac{EI_t}{EI} = \frac{E_t}{E} = \begin{cases} 1 & \text{for} \quad \frac{P}{P_y} \le a_y \\ \frac{1-\frac{P}{P_y}}{1-a_y} & \text{for} \quad \frac{P}{P_y} > a_y \end{cases} \tag{11}$$

where $a_y = 0.8$.

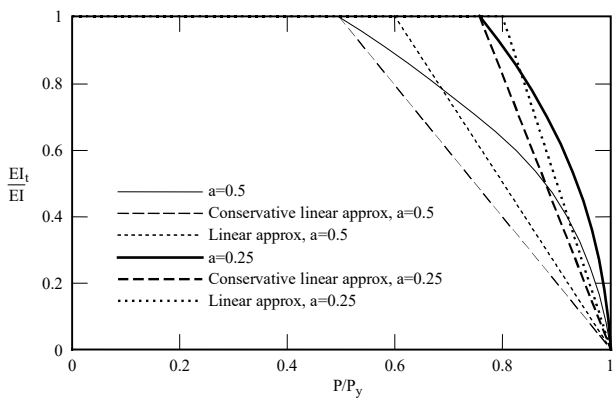

Fig. 13: Stiffness reduction curves for a=0.25 and a=0.5

4. Slenderness reduction factor (τ_b)

Equations (4) and (11) provide expressions for the stiffness reductions (EI_t/EI) resulting from sectional buckling and yielding due to residual stresses, respectively. They apply to slender and stocky CFS cross-sections, respectively, as shown in Figs 11a and 11b. Note that for stocky sections, the stiffness reduction starts at a fraction of the yield load (P_y), whereas for slender cross-sections, the

stiffness reduction starts at a fraction of the critical sectional elastic buckling load, exemplified as $P_{cr,l}$ in Fig. 11a, rather than at a fraction of the sectional strength P_{ns}.

The stiffness reductions (EI_t/EI) correspond to the stiffness reduction factor (τ_b) in Section C of the AISI-S100 Specification. The stiffness reduction may be triggered by local or distortional buckling, or by premature yielding caused by residual stresses, and hence starts at the minimum of the loads $a_l P_{cr,l}$, $a_d P_{cr,d}$ and $a_y P_y$,

$$P_s = \min\left(a_l P_{cr,l}, a_d P_{cr,d}, a_y P_y\right) \tag{12}$$

where $a_l = 0.9$, $a_d = 0.8$ and $a_y = 0.8$.

The stiffness is reduced to zero when the section capacity P_{ns} is reached, which is the minimum of the local (P_{nl}) and distortional (P_{nd}) buckling strengths,

$$P_{ns} = \min\left(P_{nl}, P_{nd}\right), \tag{13}$$

and equals the yield load P_y for sections not affected by sectional buckling. It follows that the stiffness reduction can be expressed as,

$$\tau_b = \begin{cases} 1 & \text{for} \quad P \le P_s \\ \frac{1-\frac{P}{P_{ns}}}{1-\frac{P_s}{P_{ns}}} & \text{for} \quad P > P_s \end{cases} . \tag{14}$$

To elucidate this equation, consider a cross-section whose strength is affected by local buckling but not distortional buckling. The local buckling strength P_{nl} may be determined using the Direct Strength Method [12] and calculating the slenderness at the yield load,

$$\lambda_l = \sqrt{\frac{P_y}{P_{cr,l}}} , \tag{15}$$

i.e.,

$$P_{nl} = \begin{cases} P_y & \text{for} \quad \lambda_l \le 0.776 \\ \left[1 - 0.15\left(\frac{P_{cr,l}}{P_y}\right)^{0.4}\right]\left(\frac{P_{cr,l}}{P_y}\right)^{0.4} P_y & \text{for} \quad \lambda_l > 0.776 \end{cases} \tag{16}$$

Local buckling will start the stiffness reduction before yielding when $a_l P_{cr,l} < a_y P_y$. In terms of local buckling slenderness (Eq. (15)), this implies that local buckling controls the initiation of stiffness reduction when the local buckling slenderness exceeds the "cross-over" slenderness ($\lambda_{c\text{-}o}$) defined by,

$$a_l F_{cr,l} = a_y F_y \quad \Rightarrow \quad \lambda_{c-o} = \sqrt{\frac{a_l}{a_y}} = 1.061 \tag{17}$$

It follows that stiffness reduction starts at $P = a_y P_y$ when $\lambda_l < \lambda_{c\text{-}o}$, and at $P = a_l P_{cr,l}$ when $\lambda_l > \lambda_{c\text{-}o}$, where $\lambda_{c\text{-}o} = 1.061$. In the slenderness range, $0.776 < \lambda_l < \lambda_{c\text{-}o}$, the section capacity P_{nl} is less than the yield load, as per Eq. (16). Thus, three ranges of slenderness are required for determining the limiting stresses for the slenderness reduction:

- Stocky sections, $\lambda_l < 0.776$: Stiffness reduction starts at $a_y P_y$ and finishes at P_y
- Intermediate slenderness sections, $0.776 < \lambda_l < \lambda_{c\text{-}o}$: Stiffness reduction starts at $a_y P_y$ and finishes at P_{ns}

- Slender sections, $\lambda_l > \lambda_{c\text{-}o}$: Stiffness reduction starts at $a_l P_{cr,l}$ and finishes at P_{ns}

The three ranges are illustrated in Fig. 14.

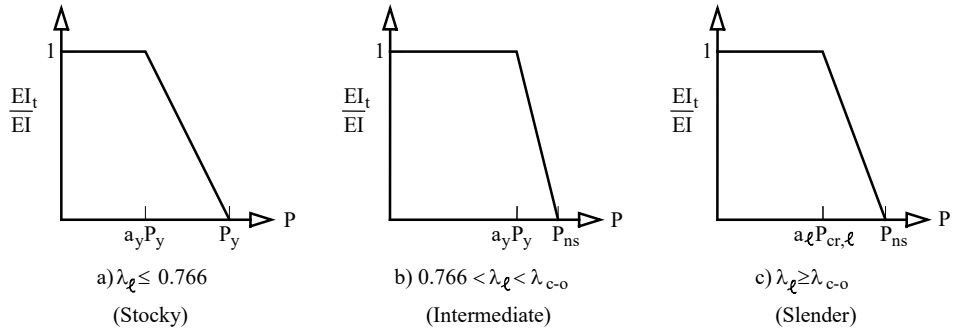

Fig. 14: Stiffness reduction curves (τ_b=EI_t/EI) for stocky, intermediate and slender cross-sections prone to local buckling

Many practical CFS cross-sections fall in the intermediate slenderness range. In the slender range, the stiffness reduction starts at $a_l P_{cr,l}$ and hence is a function of slenderness (λ_l). Figure 15 shows slenderness curves for different values of slenderness for the values of $a_y = 0.8$ and $a_l = 0.9$.

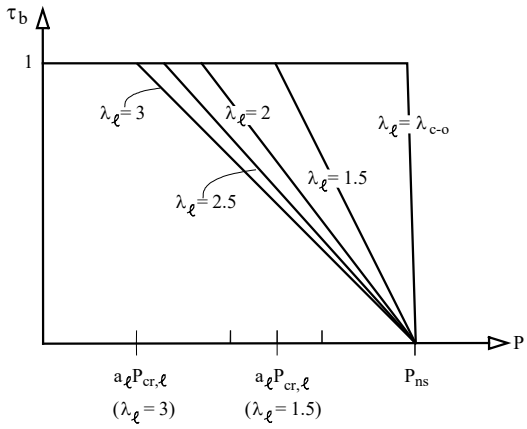

Fig. 15: Stiffness reduction curves (τ_b=EI_{eff}/EI) for slender cross-sections ($\lambda_l > \lambda_{c\text{-}o}$); a_y=0.8 and a_l=0.9

Similar curves can be constructed for sections with the distortional mode as the critical sectional buckling mode. In this case, $\lambda_{c\text{-}o} = \sqrt{a_d/a_y} = 1$, and the strength reduction starts at $\lambda_d = 0.561$ [12].

5. Conclusions

Equation (14) has been derived for calculating the stiffness reduction factor (τ_b) to be applied to the flexural and torsional rigidities of members of cold-formed steel frames when determining internal actions using beam-type geometric nonlinear elastic analysis. The Equation is in a format suitable for use in the North American specification for cold-formed steel structures, AISI-S100. The derivation of the stiffness reduction factor accounts for the gradual change of stiffness caused by geometric imperfections and residual stresses. Attention is paid to determining the initiation points for the stiffness reduction applicable to geometric imperfections in the shapes of the local and distortional buckling modes and to premature yielding induced by residual stress. The initiation points are based on measurements of geometric imperfections and decomposition of these into the buckling modes of the member. Likewise, the initiation point for stiffness reduction caused by residual stresses is based on measurements of residual stress in cold-rolled sections.

References

1. Bijlaard, P. and G. Fisher, Column Strength of H-sections and Square Tubes in Postbuckling Range of Component Plates, TN2994. 1953, NACA: Washington, D.C.
2. Graves Smith, T.R., The ultimate strength of locally buckled columns of arbitrary length, Proceedings, Symposium on Thin-walled Structures, in Thin-walled Structures, K.C. Rockey and H.V. Hill, Editors. 1969, Crosby-Lockwood: Swansea. p. 35-60.
3. Hancock, G.J., Interaction buckling in I-section columns. Journal of the Structural Division, American Society of Civil Engineers, 1981. **107**(ST1): p. 165-179.
4. Rasmussen, K.J.R., Bifurcation of locally buckled members. Thin-Walled Structures, 1997. **28**(2): p. 117-154.
5. Young, B. and K.J.R. Rasmussen, Inelastic bifurcation of cold-formed singly symmetric columns. Thin-Walled Structures, 2000. **36**(3): p. 213-230.
6. Young, B. and K.J.R. Rasmussen, Bifurcation of singly symmetric columns. Thin-Walled Structures, 1997. **28**(2): p. 155-177.
7. Rasmussen, K.J.R., Bifurcation of locally buckled point symmetric columns - Analytical developments. Thin-Walled Structures, 2006. **44**(11): p. 1161-1174.
8. Rasmussen, K.J.R. and A.S. Hasham, Flexural and flexural-torsional bifurcation of locally buckled beam-columns. Thin-Walled Structures, 1997. **29**(1-4): p. 203-233.
9. Surovek, A.E., Advanced Analysis in Steel Frame Design: Guidelines for Direct Second-order Inelastic Analysis, in Special Project Committee on Advanced Analysis of the Technical Committee on Structural Members of the Structural Engineering Institute of ASCE. 2011, American Society of Civil Engineers.
10. Yao, Y., W.-M. Quach, and B. Young, Finite element-based method for residual stresses and plastic strains in coldformed steel hollow sections. Engineering Structures, 2019. **188**: p. 24–42.
11. AISC-360, Specification for Structural Steel Buildings. 2016, American Institute of Steel Construction: Chicago.
12. AISI-S100, North American Specification for the Design of Cold-formed Steel Structural Members. 2016, American Iron and Steel Institute: Washington, D.C.
13. AISC-360, Specification for Structural Steel Buildings, (July 2022 draft). 2022, American Institute of Steel Construction: Chicago.
14. Silvestre, N. and D. Camotim, Local-plate and distortional postbuckling behavior of cold-formed steel lipped channel columns with intermediate stiffeners. Journal of Structural Engineering, American Society of Civil Engineers, 2006. **132**(4): p. 529-540.
15. Schafer, B.W. and T. Pekoz, Computational modeling of cold-formed steel: characterizing geometric imperfections and residual stresses. Journal of Constructional Steel Research, 1998. **47**: p. 193-210.
16. Zeinoddini, V.M. and B.W. Schafer, Simulation of geometric imperfections in cold-formed steel members using spectral representation approach. Thin-Walled Structures, 2012. **60**: p. 105-117.
17. Rasmussen, K.J.R. and G.J. Hancock, Geometric imperfections in plated structures subject to interaction between buckling modes. Thin-Walled Structures, 1988. **6**(6): p. 433-452.
18. Key, P.W. and G.J. Hancock, A theoretical investigation of the column behaviour of cold-formed square hollow sections. Thin-Walled Structures, 1993(**16**): p. 31-64.
19. Liu, W., K.J.R. Rasmussen, and H. Zhang, Modelling and probabilistic study of the residual stress of cold-formed hollow steel sections. Engineering Structures, 2017. **150**: p. 986–995.
20. Ma, J.-L., T.-M. Chan, and B. Young, Material properties and residual stresses of cold-formed high strength steel hollow sections. Journal of Constructional Steel Research, 2015. **109**: p. 152-165.